

Article

Selective and Efficient Reduction of Nitrate to Gaseous Nitrogen from Drinking Water Source by UV/Oxalic Acid/Ferric Iron Systems: Effectiveness and Mechanisms

Zhiyuan Shi ¹, Falu Wang ^{2,3,4}, Qian Xiao ^{2,3,*}, Shuili Yu ^{2,3,*} and Xingli Ji ^{2,3}

¹ SIIIC Environment Holdings Ltd., Shanghai 200021, China; shizhiyuan@siic.com

² State Key Laboratory of Pollution Control and Resource Reuse, College of Environmental Science and Engineering, Tongji University, Siping Campus, Shanghai 200092, China; wangfalu@smedi.com (F.W.); jixingli@tongji.edu.cn (X.J.)

³ Shanghai Institute of Pollution Control and Ecological Security, Siping Campus, Shanghai 200092, China

⁴ Shanghai Municipal Engineering Design Institute (Group) Co., Ltd., Shanghai 200092, China

* Correspondence: 2015xiaoqian@tongji.edu.cn (Q.X.); ysl@tongji.edu.cn (S.Y.);
Tel./Fax: +86-21-6598-2708 (Q.X. & S.Y.)



Citation: Shi, Z.; Wang, F.; Xiao, Q.; Yu, S.; Ji, X. Selective and Efficient Reduction of Nitrate to Gaseous Nitrogen from Drinking Water Source by UV/Oxalic Acid/Ferric Iron Systems: Effectiveness and Mechanisms. *Catalysts* **2022**, *12*, 348. <https://doi.org/10.3390/catal12030348>

Academic Editors: Ran Du, Chengzhou Zhu, Bin Cai, Wei Liu, Dan Wen, Alexander Eychmüller and Patrick Da Costa

Received: 25 January 2022

Accepted: 16 March 2022

Published: 18 March 2022

Publisher's Note: MDPI stays neutral with regard to jurisdictional claims in published maps and institutional affiliations.



Copyright: © 2022 by the authors. Licensee MDPI, Basel, Switzerland. This article is an open access article distributed under the terms and conditions of the Creative Commons Attribution (CC BY) license (<https://creativecommons.org/licenses/by/4.0/>).

Abstract: Nitrate (NO_3^-) reduction in water has been receiving increasing attention in water treatment due to its carcinogenic and endocrine-disrupting properties. This study employs a novel advanced reduction process, the UV/oxalic acid/ferric iron systems ($\text{UV}/\text{C}_2\text{O}_4^{2-}/\text{Fe}^{3+}$ systems), in reducing NO_3^- due to its high reduction efficiency, excellent selectivity, and low treatment cost. The $\text{UV}/\text{C}_2\text{O}_4^{2-}/\text{Fe}^{3+}$ process reduced NO_3^- with pseudo-first-order reaction rate constants of $0.0150 \pm 0.0013 \text{ min}^{-1}$, minimizing 91.4% of 60 mg/L NO_3^- and reaching 84.2% of selectivity for gaseous nitrogen after 180 min at pH_{ini} . 7.0 and 0.5 mg/L dissolved oxygen (DO). Carbon dioxide radical anion ($\text{CO}_2^{\bullet-}$) played a predominant role in reducing NO_3^- . Gaseous nitrogen and NH_4^+ , as well as CO_2 , were the main nitrogen- and carbon-containing products, respectively, and reduction pathways were proposed accordingly. A suitable level of oxalic acids (3 mM) and NO_3^- (60 mg/L) was recommended; increasing initial iron concentrations and UV intensity increased NO_3^- reduction. Instead, increasing the solution pH decreased the reduction, and 0.5–8.0 mg/L DO negligibly affected the process. Moreover, $\text{UV}/\text{C}_2\text{O}_4^{2-}/\text{Fe}^{3+}$ systems were not retarded by 0.1–10 mM SO_4^{2-} or Cl^- or 0.1–1.0 mM HCO_3^- but were prohibited by 10 mM HCO_3^- and 30 mg-C/L humic acids. There was a lower reduction of NO_3^- in simulated groundwater (72.8%) than deionized water after 180 min at pH_{ini} . 7.0 and 0.5 mg/L DO, which meets the drinking water standard (<10 mg/L N- NO_3^-). Therefore, $\text{UV}/\text{C}_2\text{O}_4^{2-}/\text{Fe}^{3+}$ systems are promising approaches to selectively and efficiently reduce NO_3^- in drinking water.

Keywords: advanced reduction processes; carbon dioxide radical anion; drinking water; gaseous nitrogen selectivity; nitrate reduction

1. Introduction

Nitrate (NO_3^-) naturally exists in some geological formations and groundwater. It should be noted that NO_3^- contamination mainly results from anthropogenic activities, such as fertilizer runoff in farmland, rainwater runoff on the urban surface, and the discharge of sewage or treated wastewater [1]. NO_3^- causes adverse effects to human health, such as known methemoglobinemia, carcinogens, and endocrine disruptors [2–4]. To minimize its adverse health effects, the World Health Organization has set the guideline of 50 mg/L NO_3^- (~11 mg/L as N- NO_3^-) in drinking water [1]. The United States Environmental Protection Agency (US EPA) and China, however, have regulated more stringent levels of NO_3^- at 10 mg/L N- NO_3^- [2]. Furthermore, China has also promulgated an acceptable level of ≤ 10 and ≤ 20 mg/L of N- NO_3^- , in level I and level II water sources,

respectively. As reported, NO_3^- concentrations can reach up to 300 mg/L in the drinking water and groundwater of Northern China [5]. Since NO_3^- is a stable, highly mobile, and highly soluble oxyanion, it further underscores the importance of NO_3^- reduction.

Currently, there are several major technologies for minimizing NO_3^- , including biological methods [6,7], catalytic reduction [8], electrocatalysis [9,10], photocatalysis [11,12], and membrane technologies [13]. Although reverse osmosis has already been implemented in a practical process [14], its development has been limited due to its large investment costs and high operating expenses. The other existing technologies mentioned above have been barely promoted and applied in actual water treatment systems. On the contrary, photocatalysis has received much attention due to its high performance, excellent stability, and easier combination with ultraviolet illumination, primarily including homogeneous and heterogeneous photocatalytic processes [15–18]. Furthermore, reducing radicals, such as aqueous electrons (e_{aq}^-) and carbon dioxide radical anions ($\text{CO}_2^{\bullet-}$), is responsible for the photocatalytic system [19]. Admittedly, e_{aq}^- -based systems can highly effectively decompose various contaminants at nearly diffusion-limited rates (10^9 – $10^{10} \text{ M}^{-1} \text{ s}^{-1}$) [20–22] because of their very high reduction potential (e.g., -2.9 V vs. standard hydrogen electrode (SHE) for e_{aq}^-), including bromate [20,23], perchlorate [24,25], chlorate [26], nitrate [27], and halogenated organic compounds [28,29]. However, they have low selectivity and thus can be largely affected by competing background compounds in real water. These further suggest their low potential for practical applications.

On the other hand, $\text{CO}_2^{\bullet-}$ is generally formed from different hole scavengers and is a very strong one-electron reductant with a high reduction potential of $E^0(\text{CO}_2/\text{CO}_2^{\bullet-}) = -1.81 \text{ V}$ vs. SHE [19]. The $\text{CO}_2^{\bullet-}$ -related process has recently received considerable attention for water environmental remediation, i.e., efficiently removing a wide range of pollutants, including trichloroacetic acid [30], carbon tetrachloride [31], hexavalent chromium [32], divalent mercury [33], nitrate [34], etc. Although the formate-radical-induced photochemical process could efficiently remove NO_3^- , it requires larger formic acid doses and also likely produces toxic and harmful products, such as formic acid. Reportedly, An et al. [35] found that $\text{CO}_2^{\bullet-}$ generated from Fe(III)/oxalate/UV systems played a predominant role in the effective reduction of nitrite to N_2 . Additionally, there is a high likelihood that the Fe(III)/oxalate/UV systems could selectively reduce NO_3^- without decreasing the decontamination rate. To the best of our knowledge, there has been no report of the UV/ $\text{C}_2\text{O}_4^{2-}/\text{Fe}^{3+}$ process reducing NO_3^- in water under neutral conditions. Therefore, we employed the $\text{CO}_2^{\bullet-}$ -associated process, Fe(III)/oxalic acid/UV systems (UV/ $\text{H}_2\text{C}_2\text{O}_4/\text{Fe}^{3+}$ systems), in the treatment of NO_3^- in drinking water, mainly because they have less involvement with reactants, efficient NO_3^- removal, and promote further formation of innocuous products, including CO_2 and iron precipitates.

In this work, the efficiency of NO_3^- reduction and gaseous nitrogen conversion was first carried out in circumneutral environments in the UV/ $\text{H}_2\text{C}_2\text{O}_4/\text{Fe}^{3+}$ process. We further investigated the effects of important operating parameters, i.e., initial concentrations of oxalic acids and iron dosage, initial nitrate levels, solution pH, UV intensity, and dissolved oxygen, as well as background compounds, i.e., chloride, sulfate, hydrocarbonate, and organic matters. The mechanism of NO_3^- reduction was carried out in the UV/ $\text{H}_2\text{C}_2\text{O}_4/\text{Fe}^{3+}$ system. Reduction pathways of NO_3^- were proposed accordingly. Finally, the reduction kinetics of NO_3^- was investigated in simulated groundwater to verify the effectiveness of UV/ $\text{H}_2\text{C}_2\text{O}_4/\text{Fe}^{3+}$ systems in actual water.

2. Experimental Section

2.1. Materials

Potassium nitrate (KNO_3 , ≥99.0%), iron(III) chloride (FeCl_3 , ≥97.0%), nitrate nitrite (NaNO_2 , ≥99.0%), oxalic acid ($\text{H}_2\text{C}_2\text{O}_4$, 98.0%), sodium hydroxide (NaOH , ≥96.0%), hydrogen chloride (HCl , 36.0–38.0%), sodium sulfate (Na_2SO_4 , ≥99.0%), sodium chloride (NaCl , ≥99.8%), sodium hydrogen carbonate (NaHCO_3 , ≥99.5%), calcium chloride (CaCl_2 , ≥96.0%), magnesium sulfate (MgSO_4 , ≥98.0%), potassium iodide, (KI , ≥99.0%), potas-

sium iodate (KIO_3 , $\geq 99.8\%$), humic acid (HA), and Nessler's reagent were obtained from Sinopharm Chemical Reagent Co. Ltd. (Shanghai, China). Most chemicals were at least of analytical grade and used as received. All solutions were prepared in Milli-Q ultra-pure water ($18.2 \text{ M}\Omega \text{ cm}$, Millipore). The simulated groundwater was utilized for testing the performance of UV/ $\text{H}_2\text{C}_2\text{O}_4/\text{Fe}^{3+}$ systems. The major characteristics of simulated groundwater, which were nearly the same as the components of realistic groundwater, are summarized in Table S1.

2.2. Experimental Procedures

The photoreactor and methodology for irradiation experiments have been depicted elsewhere [23,36]. Generally, we selected a medium-pressure mercury UV lamp (UV-M) (500 W, Xujiang Electromechanical Plant, Nanjing, China). The UV irradiation intensity was estimated to be 10.2 mW/cm^2 .

Prior to photocatalytic reduction experiments, the photoreactor was preheated for about 15 min to achieve stabilization. Meanwhile, stock solutions of KNO_3 (6 g/L), FeCl_3 (5 mM), $\text{H}_2\text{C}_2\text{O}_4$ (300 mM), Na_2SO_4 (10 or 100 mM), NaCl (10 or 100 mM), NaHCO_3 (10 or 100 mM), and HA (100 mg/L) were prepared. Magnetic stirring was utilized for the complete mixing of the solution. Reductive reactions were initiated by adding KNO_3 , FeCl_3 , and $\text{H}_2\text{C}_2\text{O}_4$ in aqueous solutions to a quartz tube. Samples were then taken at regulated time intervals, including 0, 20, 40, 60, 80, 100, 120, and 180 min, and immediately analyzed for N-containing compounds (i.e., NO_3^- , NO_2^- , NH_4^+ , and Total N (TN)), residual DOC, and iron ion levels. Furthermore, the impact of important variables on NO_3^- reduction was determined for the UV/ $\text{C}_2\text{O}_4^{2-}/\text{Fe}^{3+}$ systems by varying initial concentrations of oxalic acid (1–6 mM), ferric iron (0–0.1 mM), and NO_3^- (20–100 mg NO_3^- /L) and varying the solution pH (3–11) and UV lamp power (100, 300, and 500 W), as well as dissolved oxygen level (0.5 and 8.0 mg/L). Moreover, to determine the application potential, the reduction of NO_3^- was investigated in simulated groundwater for an initial concentration of 120 mg NO_3^- /L in the UV/ $\text{H}_2\text{C}_2\text{O}_4/\text{Fe}^{3+}$ process. Additionally, a $\text{CO}_2\bullet^-$ -quenching experiment was conducted to confirm the predominant species in the process. All experiments were performed in a photoreactor, as illustrated in Figure 1.

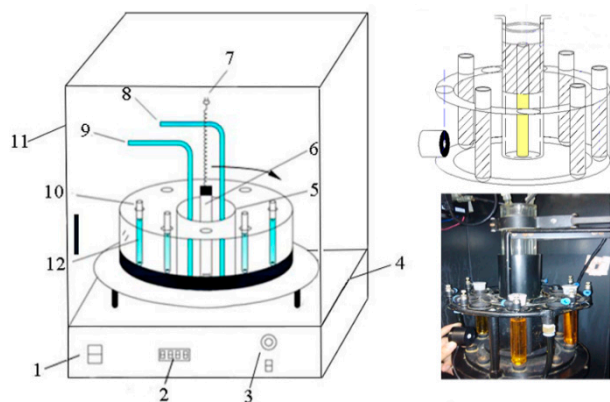


Figure 1. Schematic illustration of photoreactor. (1. rotary button; 2. temperature display; 3. magnetic stirrer button; 4. lampstand; 5. quartz vessel; 6. UV lamp; 7. power plug; 8. cooling water inlet; 9. cooling water outlet; 10. quartz tube reactor; 11. cover; and 12. reaction solution).

Unless otherwise noted, the initial NO_3^- concentration was 60 mg NO_3^- /L, representing NO_3^- levels (60–70 mg NO_3^- /L) in water from a reservoir in Qingdao, China. The solution temperature was maintained at $25 (\pm 0.5)^\circ\text{C}$. The initial solution pH was adjusted using either 0.1 mM HCl or NaOH to 3.0, 5.0, 7.0, 9.0, and 11.0 in different experiments. All experiments proceeded without adding a buffer solution to simulate practical water treatment processes. The corresponding variation in solution pH was monitored over time, which indicated an actual water treatment process. Dissolved oxygen (DO) was used in

concentrations of 0.5 and 8.0 mg/L with and without purging using nitrogen gas for about 60 min. All experiments were repeated in triplicate independently, and average values along with the standard deviation are presented.

2.3. Chemical Analysis

Solution pH was determined with a pH meter (LA-pH 10, HACH, Loveland, CO, USA), and DO concentrations were measured with a DO meter (HQ30d, HACH, Loveland, CO, USA). Dissolved organic carbon (DOC) and the total nitrogen (TN) were analyzed by a TOC analyzer (TOC-L, Shimadzu, Kyoto, Japan). The ferrous ion concentration was immediately measured without filtering by the 1,10-phenanthroline colorimetric method at 510 nm using an ultraviolet-visible spectrophotometer (HACH DR1900, Loveland, CO, USA) [37]. According to our previous study, there were no significant differences in Fe(II) levels without and with filtration [38]. Inorganic anions (NO_3^- and NO_2^-) were quantified using an ion chromatograph (Dionex ICS-1000, Sunnyvale, CA, USA) equipped with a Dionex AS19 analytical column (4×250 mm) and an AG19 guard column (4×50 mm) for analysis of NO_3^- and NO_2^- . Potassium hydroxide at a concentration of 20 mM was utilized as an effluent in an equal washing mode. Furthermore, a flow rate of 1.0 mL/min, a constant suppressor current of 50 mM, a column temperature of 30 °C, an inlet ring of 25 µL, and a duration of 25 min were set during the measurement. Of note, all samples were filtered using 0.22 µm membrane filters (Nylon, Titan) before the analysis of ion chromatography. Ammonium ion (N-NH_3) was further measured by UV-vis spectrophotometer (DR6000, HACH, USA), with a measurement range from 0.02 to 2.50 mg/L N-NH_3 .

3. Results and Discussion

3.1. Photocatalytic Reduction Efficiency of Nitrate and Gaseous Nitrogen Selectivity

Figure 2 shows the reduction efficiency of NO_3^- in UV/ $\text{C}_2\text{O}_4^{2-}/\text{Fe}^{3+}$ systems. As expected, UV irradiation alone and UV/ Fe^{3+} systems reduced NO_3^- by 24.3% and 25.0%, respectively, within 180 min. In contrast, NO_3^- was effectively reduced (removal efficiency = 41.3%) after a reaction time of 180 min in the UV/ $\text{C}_2\text{O}_4^{2-}$ process as shown in Figure 2a. Comparatively, a more rapid reduction in NO_3^- levels was also observed within 180 min with a removal efficiency of 91.4% for an initial NO_3^- concentration of 60 mg/L in the UV/ $\text{C}_2\text{O}_4^{2-}/\text{Fe}^{3+}$ systems (Figure 2a), which was larger than in previous studies (i.e., removal efficiency = 92.4% in 6 h) [39,40]. Furthermore, the reduction of NO_3^- follows the pseudo-first-order decay kinetics as presented in Figure 2b, where the $\ln(\text{C}_0/\text{C})$ value is proportional to the reaction time. Figure 2c shows that the reaction rate constants for 180 min in the UV/ $\text{C}_2\text{O}_4^{2-}/\text{Fe}^{3+}$ process, UV/ $\text{C}_2\text{O}_4^{2-}$ systems, UV/ Fe^{3+} systems, and UV alone were 0.0150 ± 0.0013 , 0.0034 ± 0.0007 , 0.0015 ± 0.0003 , and $0.0015 \pm 0.0002 \text{ min}^{-1}$, respectively. The first-order reaction rate constant for the UV/ $\text{C}_2\text{O}_4^{2-}/\text{Fe}^{3+}$ process was 3.4 and 5.2 times greater than that for the UV/ $\text{SiW}_9/\text{TiO}_2/\text{Cu}$ and UV/ TiO_2 systems, respectively (0.0044 and 0.0029 min^{-1} , respectively) [39]. At the same time, conversion of gaseous nitrogen was carried out in the following experiments. As illustrated in Figure 3, the removal of total nitrogen (TN) reached 84.2%, implying that a large amount of NO_3^- was selectively converted to gaseous nitrogen, thus showing its high application potential.

Notably, $\text{C}_2\text{O}_4^{2-}$ addition probably led to subsequent pollution problems. Thus, we further investigated variations in TOC with reaction time to confirm the effect of $\text{C}_2\text{O}_4^{2-}$ levels on this process. Results show TOC approaching zero with removal efficiencies of 100% after 120 min in Figure S1, indicating that the C-containing secondary contamination could be nearly completely removed by managing doses of oxalic acids. Taking together, UV/ $\text{C}_2\text{O}_4^{2-}/\text{Fe}^{3+}$ systems could be an alternative technique for selective and efficient reduction of NO_3^- in water.

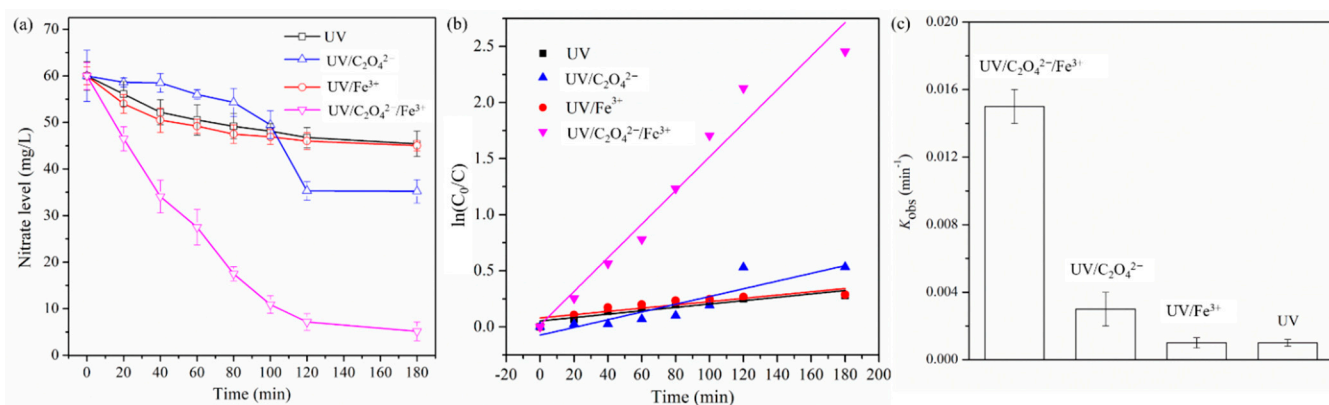


Figure 2. (a) Reduction kinetics of NO_3^- in the $\text{UV}/\text{C}_2\text{O}_4^{2-}/\text{Fe}^{3+}$ systems, (b) the $\ln(\text{C}_0/\text{C})$ versus reaction time, and (c) their pseudo-first-order rate constants (k). Experimental conditions: $[\text{NO}_3^-]_0 = 60 \text{ mg/L}$, $[\text{C}_2\text{O}_4^{2-}]_0 = 3 \text{ mM}$, $[\text{Fe}^{3+}]_0 = 0.05 \text{ mM}$, $I_0 = 10.2 \text{ mW/cm}^2$ (wavelength = 365 nm), $[\text{DO}]_0 = 0.5 \pm 0.1 \text{ mg/L}$, $\text{pH}_{\text{ini.}} = 7.0 \pm 0.2$, and $T = 25 \pm 0.5 \text{ }^\circ\text{C}$. Error bars represent the standard deviation from three experiments.

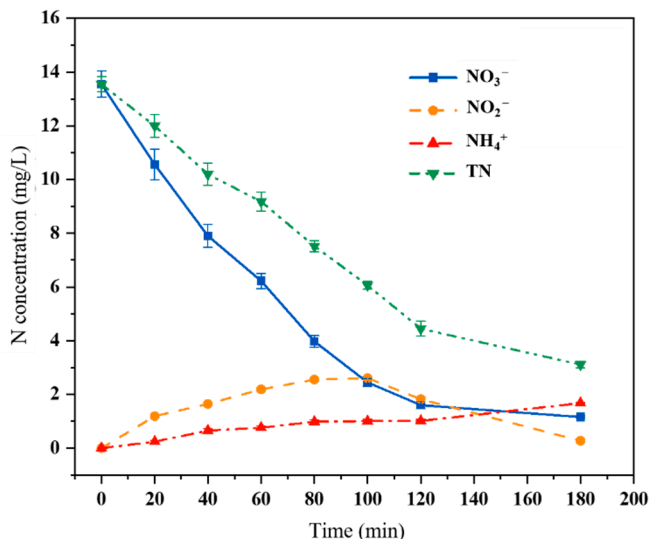


Figure 3. Formation of primary products during reduction of NO_3^- in the $\text{UV}/\text{C}_2\text{O}_4^{2-}/\text{Fe}^{3+}$ systems. Experimental conditions: $[\text{NO}_3^-]_0 = 60 \text{ mg/L}$, $[\text{C}_2\text{O}_4^{2-}]_0 = 3 \text{ mM}$, $[\text{Fe}^{3+}]_0 = 0.05 \text{ mM}$, $I_0 = 10.2 \text{ mW/cm}^2$ (wavelength = 365 nm), $[\text{DO}]_0 = 0.5 \pm 0.1 \text{ mg/L}$, $\text{pH}_{\text{ini.}} = 7.0 \pm 0.2$, and $T = 25 \pm 0.5 \text{ }^\circ\text{C}$. Error bars represent the standard deviation from three experiments. Error bars smaller than symbols are not visible.

3.2. The Effect of Important Parameters

Figure 4a shows the effect of initial oxalic acid concentrations. Obviously, an initial dose of oxalic acids facilitated the reduction of NO_3^- in the $\text{UV}/\text{C}_2\text{O}_4^{2-}/\text{Fe}^{3+}$ systems. For example, there was a minor removal observed even for an initial $\text{C}_2\text{O}_4^{2-}$ level of 1 mM after 180 min, which we attributed to UV irradiation, as evidenced by the results shown in Figure 2a. The efficiency of NO_3^- reduction was enhanced by increasing the initial $\text{H}_2\text{C}_2\text{O}_4$ concentration, and then declined after a further improvement in $\text{H}_2\text{C}_2\text{O}_4$ levels. The optimal reduction efficacy was obtained at 3 and 4 mM $\text{H}_2\text{C}_2\text{O}_4$ during the $\text{UV}/\text{C}_2\text{O}_4^{2-}/\text{Fe}^{3+}$ process, probably because an appropriate addition of $\text{H}_2\text{C}_2\text{O}_4$ led to the largely formed reductants and thus increased reduction. On the contrary, excessive $\text{H}_2\text{C}_2\text{O}_4$ doses resulted in a faster reducing radical-quenching reaction (Equations (1)–(3)) [41] and inhibitory NO_3^- reduction in water accordingly. These together suggest reducing $\text{CO}_2\bullet^-$ radicals probably facilitated NO_3^- reduction during the $\text{UV}/\text{C}_2\text{O}_4^{2-}/\text{Fe}^{3+}$ process.

Furthermore, to confirm the effect of oxalic acid concentrations on NO_3^- reduction, we investigated the variation in its decomposition products over time in the UV/ $\text{C}_2\text{O}_4^{2-}/\text{Fe}^{3+}$ systems. As shown in Figure S2, efficiencies of NO_3^- reduction reached 28.7%, 62.1%, 91.4%, 95.0%, 92.3%, and 71.3% with doses of 1, 2, 3, 4, 5, and 6 mM $\text{H}_2\text{C}_2\text{O}_4$, respectively; simultaneously, the conversion efficiency of gaseous nitrogen was 22.8%, 51.1%, 84.2%, 44.3%, 36.9%, and 24.0% for initial $\text{H}_2\text{C}_2\text{O}_4$ levels of 1, 2, 3, 4, 5, and 6 mM, respectively. Clearly, the maximum selectivity to gaseous nitrogen was achieved at a dose of 3 mM $\text{H}_2\text{C}_2\text{O}_4$, which was due to the greater formation of reducing radicals. The results, therefore, imply that reducing species predominated in the selective conversion reaction of gaseous nitrogen. A total of 3 mM oxalic acid was selected in the following experiments in terms of reduction efficiencies and gaseous nitrogen selectivity.

Figure 4b shows the effect of the initial iron dosage. Generally, the higher the initial iron dosage is, the faster the reductive reaction is. After dosing Fe^{3+} , NO_3^- reduction was obviously improved during the process compared to that in the absence of Fe^{3+} , as illustrated in Figure 4b. For instance, the efficiency of NO_3^- reduction was 42.0%, 84.5%, 91.4%, 91.4%, and 93.9%, in the absence and presence of 0.017, 0.025, 0.05, and 0.1 mM, respectively, with a respective gaseous nitrogen selectivity at 43.4%, 53.4%, 62.4%, 84.2%, and 74.9% (Figure S3). Further, degradation kinetics of NO_3^- at various Fe^{3+} doses could also be well-fitted using pseudo-first-order kinetics models. The results show that the reduction rate constants were 0.010, 0.013, 0.015, and 0.017 min^{-1} at the initial Fe^{3+} levels of 0.017, 0.025, 0.05, and 0.1 mM, respectively, as shown in Table S2. These were highly consistent with the results of Equations (4)–(7), where higher Fe^{3+} doses led to a greater formation of the iron(III)–oxalate complex and thus increased production of reducing radicals such as $\text{C}_2\text{O}_4^{\bullet-}$ and $\text{CO}_2^{\bullet-}$. Accordingly, NO_3^- reduction would be improved in the UV/ $\text{C}_2\text{O}_4^{2-}/\text{Fe}^{3+}$ systems. It was interesting to find that as Fe^{3+} concentrations further increased to 0.1 mM, although NO_3^- reduction was slightly improved, the conversion of gaseous nitrogen was decreased. This might be because excessive reducing-radical (i.e., $\text{CO}_2^{\bullet-}$)-induced reactions tended to proceed towards the NH_4^+ product, as substantiated by the results shown in Figure S3. Therefore, 0.05 mM Fe^{3+} was utilized for NO_3^- reduction in UV/ $\text{C}_2\text{O}_4^{2-}/\text{Fe}^{3+}$ systems.

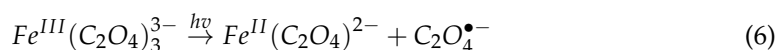
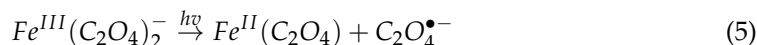
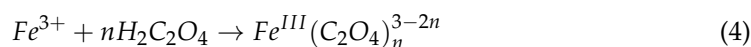
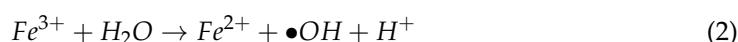


Figure 4c presents the effect of the initial solution pH. Increasing the initial pH contributed to a slower NO_3^- reduction. NO_3^- reduction reached 96.0%, 95.5%, 91.4%, 91.0%, and 87.0%, at pH_{ini} 3, 5, 7, 9, and 11 (initial NO_3^- levels = 60 mg/L), respectively, in the UV/ $\text{C}_2\text{O}_4^{2-}/\text{Fe}^{3+}$ process. The reduction kinetics of NO_3^- follows the pseudo-first-order kinetics. As presented in Figure S4 and Table S3, the reaction rate constants were determined to be 0.019, 0.018, 0.015, 0.014, and 0.012 min^{-1} at initial solution pHs of 3, 5, 7, 9, and 11, respectively. According to previously reported literature, iron–oxalate complexes varied with the initial solution pH [42]. Figure 4d further presents the distribution of iron (III)-containing compounds as a function of the solution pH. At a solution pH below 2.9, $\text{Fe}(\text{C}_2\text{O}_4)_2^-$ was the dominant species, and $\text{Fe}(\text{C}_2\text{O}_4)_3^{3-}$ became the main complex at a pH ranging from 2.9 to 6.3. As the solution pH further increased to above 6.3, the fraction of Fe_2O_3 predominated. The mole fraction of Fe_2O_3 was nearly 100% at a pH greater than

7.0 (Figure 4d). As is known, $\text{Fe}(\text{C}_2\text{O}_4)_2^{2-}$ and $\text{Fe}(\text{C}_2\text{O}_4)_3^{3-}$ can form $\text{CO}_2^{\bullet-}$, as shown by Equations (5)–(7), while Fe_2O_3 cannot produce $\text{CO}_2^{\bullet-}$. Therefore, the slower NO_3^- reduction kinetics at a higher pH was probably the consequence of the less formation of $\text{CO}_2^{\bullet-}$ resulting from the decreased fraction of $\text{Fe}(\text{C}_2\text{O}_4)_2^{2-}$ and $\text{Fe}(\text{C}_2\text{O}_4)_3^{3-}$ and increased generation of Fe_2O_3 .

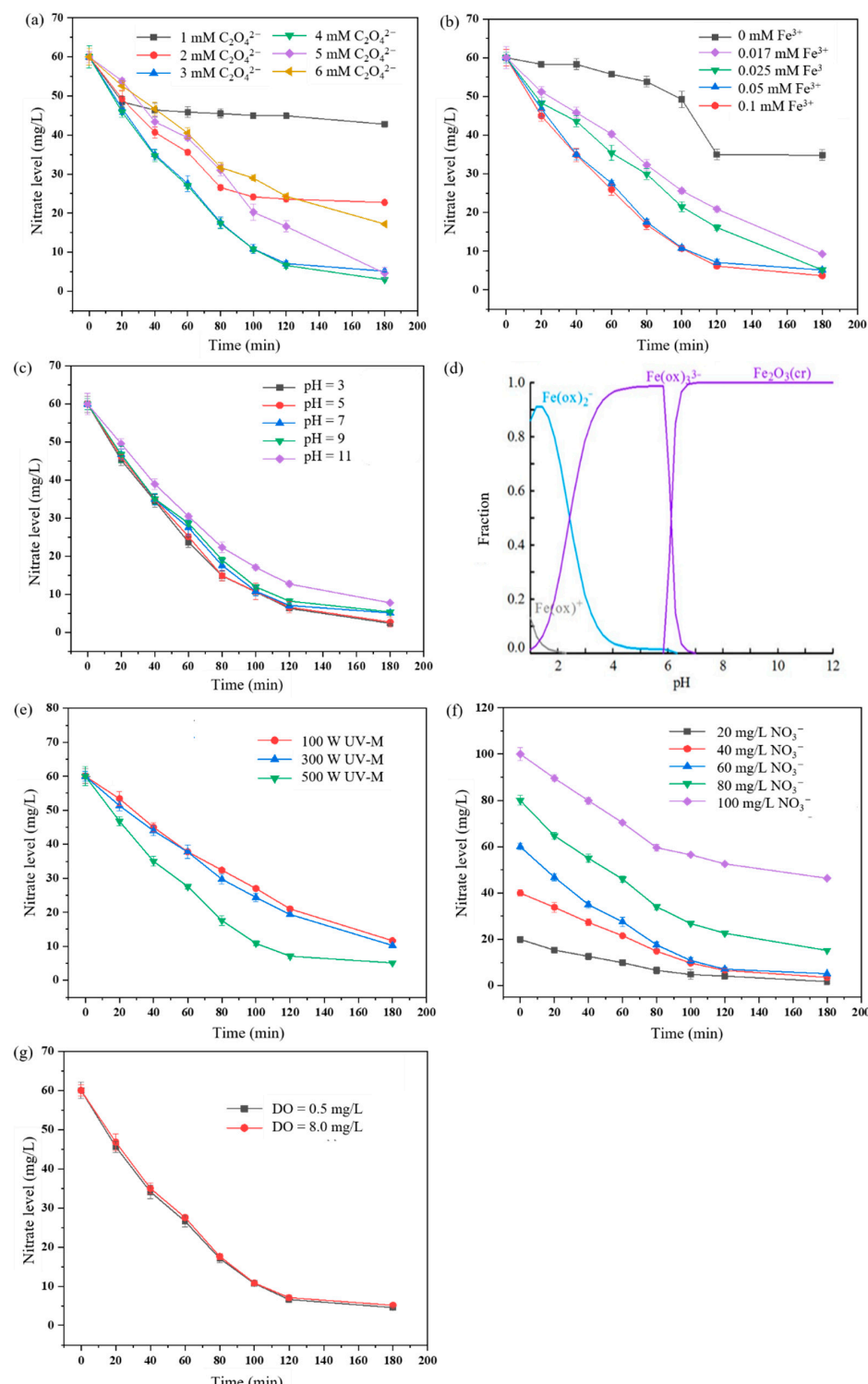


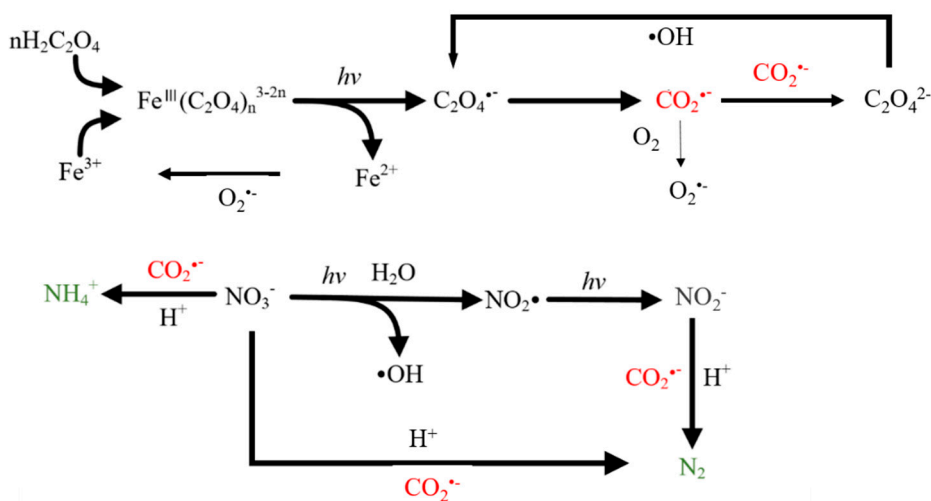
Figure 4. The effect of (a) initial oxalic acid levels, (b) initial iron dosage, (c) initial solution pH, (d) the distribution of iron–oxalate complexes at various pHs, (e) lamp power, (f) initial nitrate

concentrations, and (g) dissolved oxygen (DO) on NO_3^- reduction in the $\text{UV}/\text{C}_2\text{O}_4^{2-}/\text{Fe}^{3+}$ process. Experimental conditions: $[\text{NO}_3^-]_0 = 60 \text{ mg/L}$, $[\text{Fe}^{3+}]_0 = 0.05 \text{ mM}$, $I_0 = 10.2 \text{ mW/cm}^2$ (wavelength = 365 nm), $[\text{DO}]_0 = 0.5 \pm 0.1 \text{ mg/L}$, $\text{pH}_{\text{ini.}} = 7.0 \pm 0.2$, and $T = 25 \pm 0.5^\circ\text{C}$ in (a), $[\text{NO}_3^-]_0 = 60 \text{ mg/L}$, $[\text{H}_2\text{C}_2\text{O}_4]_0 = 3 \text{ mM}$, $I_0 = 10.2 \text{ mW/cm}^2$ (wavelength = 365 nm), $[\text{DO}]_0 = 0.5 \pm 0.1 \text{ mg/L}$, $\text{pH}_{\text{ini.}} = 7.0 \pm 0.2$, and $T = 25 \pm 0.5^\circ\text{C}$ in (b), $[\text{NO}_3^-]_0 = 60 \text{ mg/L}$, $[\text{H}_2\text{C}_2\text{O}_4]_0 = 3 \text{ mM}$, $[\text{Fe}^{3+}]_0 = 0.05 \text{ mM}$, $I_0 = 10.2 \text{ mW/cm}^2$ (wavelength = 365 nm), $[\text{DO}]_0 = 0.5 \pm 0.1 \text{ mg/L}$, and $T = 25 \pm 0.5^\circ\text{C}$ in (c), $[\text{Fe}^{3+}]_0 = 0.05 \text{ mM}$, and $[\text{H}_2\text{C}_2\text{O}_4]_0 = 3 \text{ mM}$ in (d), $[\text{NO}_3^-]_0 = 60 \text{ mg/L}$, $[\text{H}_2\text{C}_2\text{O}_4]_0 = 3 \text{ mM}$, $[\text{Fe}^{3+}]_0 = 0.05 \text{ mM}$, $[\text{DO}]_0 = 0.5 \pm 0.1 \text{ mg/L}$, $\text{pH}_{\text{ini.}} = 7.0 \pm 0.2$, and $T = 25 \pm 0.5^\circ\text{C}$ in (e), $[\text{H}_2\text{C}_2\text{O}_4]_0 = 3 \text{ mM}$, $[\text{Fe}^{3+}]_0 = 0.05 \text{ mM}$, $I_0 = 10.2 \text{ mW/cm}^2$ (wavelength = 365 nm), $[\text{DO}]_0 = 0.5 \pm 0.1 \text{ mg/L}$, $\text{pH}_{\text{ini.}} = 7.0 \pm 0.2$, and $T = 25 \pm 0.5^\circ\text{C}$ in (f), and $[\text{NO}_3^-]_0 = 60 \text{ mg/L}$, $[\text{H}_2\text{C}_2\text{O}_4]_0 = 3 \text{ mM}$, $[\text{Fe}^{3+}]_0 = 0.05 \text{ mM}$, $I_0 = 10.2 \text{ mW/cm}^2$ (wavelength = 365 nm), $[\text{DO}]_0 = 0.5 \pm 0.1 \text{ or } 8.0 \pm 0.3 \text{ mg/L}$, $\text{pH}_{\text{ini.}} = 7.0 \pm 0.2$, and $T = 25 \pm 0.5^\circ\text{C}$ in (g). Error bars represent the standard deviation from three experiments. Error bars smaller than symbols are not visible.

Figure 4e further shows the effect of UV intensity. As expected, increases in irradiation intensities led to rapid production of reducing radicals, and thus the increased reduction of NO_3^- . Specifically, the NO_3^- reduction efficiency was measured as 80.6%, 82.9%, and 91.4% for a UV power of 100, 300, and 500 W, respectively, which corresponded to 67.4%, 71.6%, and 84.2%, respectively, of gaseous nitrogen selectivity in Figure S5. The degradation kinetics of NO_3^- further follows the pseudo-first-order kinetics. As shown in Table S4, reaction rate constants were estimated to be 0.009, 0.010, and 0.015 min^{-1} , with 100, 300, and 500 W, respectively, of the UV lamp. Both $\text{CO}_2^{\bullet-}$ reduction and UV illumination itself contributed to NO_3^- reduction with a strong UV light from the medium-pressure UV lamp (UV-M), which is evidenced by the results, as seen in Figure 2. Accordingly, 500 W of UV-M was selected throughout the experiment.

Figure 4f presents the effect of initial NO_3^- levels. The higher the initial NO_3^- level is, the greater the reduction kinetics of NO_3^- is. At initial NO_3^- levels of 20, 40, 60, 80, and 100 mg/L, the NO_3^- removal efficiency was determined to be 92.5%, 91.8%, 91.4%, 80.9%, and 53.6%, respectively. Meanwhile, the conversion of gaseous nitrogen was further determined. From Figure S6, gaseous nitrogen selectivity was 28.5%, 44.4%, 84.2%, 70.6%, and 54.0% in the presence of 20, 40, 60, 80, and 100 mg/L NO_3^- , respectively, after 180 min in the $\text{UV}/\text{C}_2\text{O}_4^{2-}/\text{Fe}^{3+}$ system. Interestingly, the conversion of gaseous nitrogen increased with initial NO_3^- concentrations and declined with increases in the initial level. The highest rate was achieved at an initial NO_3^- concentration of 60 mg/L. This was probably attributable to an insufficient iron(III)-oxalate complex and thus the limited formation of $\text{CO}_2^{\bullet-}$ at higher initial NO_3^- doses. Comparatively, although a faster reduction of NO_3^- was obtained at lower initial NO_3^- levels, there was still a lower conversion rate of gaseous nitrogen in the $\text{UV}/\text{C}_2\text{O}_4^{2-}/\text{Fe}^{3+}$ process. This is in accordance with the results seen in Figure S3 as the excessive $\text{CO}_2^{\bullet-}$ -induced NO_3^- reduction reaction favorably produced products other than gaseous nitrogen. Therefore, an appropriate initial NO_3^- concentration (i.e., 60 mg/L) was recommended for the $\text{UV}/\text{C}_2\text{O}_4^{2-}/\text{Fe}^{3+}$ systems.

Figure 4g shows the effect of dissolved oxygen (DO). Clearly, DO slightly affected the reduction of NO_3^- . Specifically, the reduction efficiency of NO_3^- was measured as 92.4% and 91.4% at DO levels of 8.0 and 0.5 mg/L, respectively, in the process. Accordingly, a DO of 0.5–8.0 mg/L only had a slight impact. The results could imply that oxygen was not involved in the reduction reaction in the $\text{UV}/\text{C}_2\text{O}_4^{2-}/\text{Fe}^{3+}$ systems, and/or oxygen played a role in circular reactions in the process. According to Scheme 1, which will be discussed later, DO reacted with $\text{CO}_2^{\bullet-}$ to produce $\text{O}_2^{\bullet-}$, which was shown to further oxidize Fe^{2+} and form Fe^{3+} , thus reparticipating in the formation of the iron (III)-oxalate complex and reducing radicals. Therefore, it has been confirmed that oxygen is involved in the $\text{UV}/\text{C}_2\text{O}_4^{2-}/\text{Fe}^{3+}$ systems in a circular reaction, indicating a great application potential of $\text{UV}/\text{C}_2\text{O}_4^{2-}/\text{Fe}^{3+}$ systems in real water.



Scheme 1. Proposed pathways for reduction of NO_3^- and their product formation in the $\text{UV}/\text{C}_2\text{O}_4^{2-}/\text{Fe}^{3+}$ process.

3.3. The Photocatalytic Reduction Mechanisms

3.3.1. Involved Reducing Species

It has been reported that the carbon dioxide radical anion ($\text{CO}_2^{\bullet-}$) is most likely responsible for the reduction reaction in this process [32]. To determine the role of $\text{CO}_2^{\bullet-}$, methyl viologen (MV^{2+}) was selected as the scavenging compound to perform its inhibitory effect on NO_3^- reduction. As known, MV^{2+} exhibited a good reactivity with $\text{CO}_2^{\bullet-}$ [43,44]. Figure 5a presents the efficiency of NO_3^- reduction in the presence of 0.01, 0.1, 0.2, 0.4, 5, and 10 mM MV^{2+} , which reached 87.0%, 86.7%, 75.7%, 57.5%, 33.2%, and 24.8%, respectively, and decreased by 4.4%, 4.7%, 15.7%, 33.9%, 58.2%, and 66.6%, respectively, compared to when the MV^{2+} addition was not added (91.4%). The reduction reaction was significantly inhibited by a higher MV^{2+} concentration (i.e., ≥ 10 mM MV^{2+}), as demonstrated by Equation (8) [44]. Thereby, $\text{CO}_2^{\bullet-}$ did play a major role in the reduction of NO_3^- in $\text{UV}/\text{C}_2\text{O}_4^{2-}/\text{Fe}^{3+}$ systems. Notably, 24.8% of NO_3^- reduction in 180 min at 10 mM MV^{2+} was primarily due to the UV-M illumination, consistent with the results of UV alone (removal rates of ~24.3%), as seen in Figure 2.



As stated before, in addition to $\text{CO}_2^{\bullet-}$, iron (III)-oxalate complexes can produce Fe^{2+} with UV irradiation, which would effectively reduce Cr(VI) [32]. Accordingly, Fe^{2+} might also have an impact on NO_3^- reduction. Figure 5b presents Fe^{2+} levels at different reaction times. A sharp increase in Fe^{2+} concentrations was obtained for the first 10 min, and the generated Fe^{2+} remained at a relatively stable level with further improving reaction time. For instance, Fe^{2+} concentrations increased from 0 to 2.6 mg/L over a period of 0–10 min and reached 2.8 mg/L (0.05 mM) after a further increase in time to 60 min. Additionally, the initial Fe^{3+} dosage in the system was 2.8 mg/L (0.05 mM). Thus, iron (III)-oxalate complexes with UV illumination were completely converted into Fe^{2+} and $\text{CO}_2^{\bullet-}$ within the first 10 min. As reported, a negligible reduction of NO_3^- was achieved with Fe^{2+} alone [45], thereby excluding the role of Fe^{2+} alone in the system. Collectively, it was highly probable that $\text{CO}_2^{\bullet-}$ was the major reducing species in the $\text{UV}/\text{C}_2\text{O}_4^{2-}/\text{Fe}^{3+}$ process.

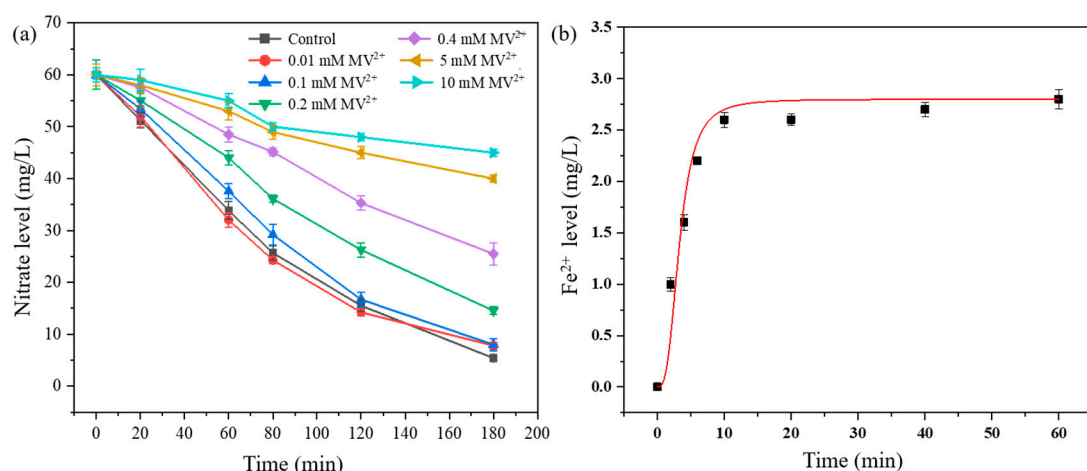


Figure 5. (a) The effect of MV²⁺ concentrations on NO₃[−] reduction and (b) time profiles of ferrous iron level in the UV/C₂O₄^{2−}/Fe³⁺ systems. Experimental conditions: [NO₃[−]]₀ = 60 mg/L, [C₂O₄^{2−}]₀ = 3 mM, [Fe³⁺]₀ = 0.05 mM, I₀ = 10.2 mW/cm² (wavelength = 365 nm), [DO]₀ = 0.5 ± 0.1 mg/L, pH_{ini.} = 7.0 ± 0.2, and T = 25 ± 0.5 °C. Error bars represent the standard deviation from three experiments.

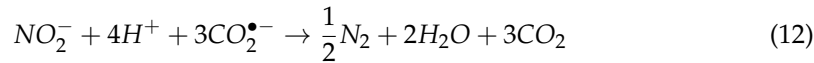
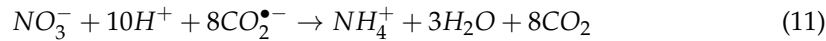
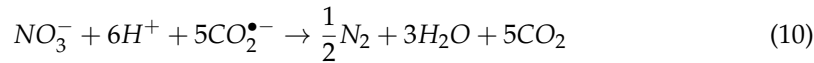
3.3.2. Formation of Products

To further investigate reduction pathways of NO₃[−] in the UV/C₂O₄^{2−}/Fe³⁺ system, the speciation of nitrogen (N) was characterized accordingly. Figure 3 presents the formation of primary products and total masses of nitrogen during NO₃[−] reduction by the UV/C₂O₄^{2−}/Fe³⁺ system. As can be seen in Figure 3, NO₃[−] levels decreased significantly with increasing reaction time. Meanwhile, the level of NH₄⁺ increased over reaction time, and NO₂[−] concentrations first increased over time but declined after a further rise in reaction time. It should be noted that the generated NO₂[−] was nearly completely minimized (100%) after 180 min, which is primarily attributable to its reaction with reducing species, i.e., reactions of NO₂[−] with the products NH₄⁺ and CO₂•[−]. Additionally, the total N content (TN) decreased over time, primarily because gaseous nitrogen was formed during the reaction process, for which N₂ was considered to be the main product due to its high reduction capacity of CO₂•[−] ($E^0(CO_2/CO_2\cdot^-) = -1.9$ V). Additionally, the TN reached 3.07 mg N/L within 180 min, which was in good accordance with the total amount of the product NH₄⁺, primarily, and the remaining NO₃[−]. These indicate that NH₄⁺ was the predominant NO₃[−] reduction product in aqueous solutions. Furthermore, as described above, almost 100% of DOC removal could be achieved after 180 min reactions, as seen in Figure S1, so carbon dioxide (CO₂) was the only oxalic acid degradation product. Accordingly, NH₄⁺, N₂, CO₂, and Fe²⁺ were the primary reaction products in the UV/C₂O₄^{2−}/Fe³⁺ systems.

3.3.3. Proposed Reduction Pathways

The transformation pathway for NO₃[−] reduction was proposed in the UV/C₂O₄^{2−}/Fe³⁺ systems in Scheme 1. In the UV/C₂O₄^{2−}/Fe³⁺ systems, the irradiation of Fe³⁺ and C₂O₄^{2−} finally led to the production of oxalate radicals, C₂O₄•[−] (Equations (1)–(3)). Additionally, C₂O₄^{2−} reacts with Fe³⁺, producing the iron(III)–oxalate complex, Fe^{III}(C₂O₄)_n^{3−2n}, as shown in Equation (4), including two main species, Fe^{III}(C₂O₄)₂[−] and Fe^{III}(C₂O₄)₃^{3−}. Subsequently, under UV irradiation, these complexes decomposed and then generated C₂O₄•[−], as shown by Equations (5) and (6). Furthermore, C₂O₄•[−] decomposed into CO₂ and CO₂•[−] according to Equation (7) [46], which is in high accordance with the results shown in Figure 4b. In addition, •OH could also react with C₂O₄^{2−} to produce C₂O₄•[−].

and finally $\text{CO}_2^{\bullet-}$, as shown in Equations (7) and (9) [46]. Of note, excessive $\text{CO}_2^{\bullet-}$ most likely recombined in pairs to generate $\text{C}_2\text{O}_4^{2-}$, as shown in Scheme 1 [41].



Three major pathways for NO_3^- reduction are proposed. On the one hand, NO_3^- was photolyzed to NO_2^\bullet and $\bullet\text{OH}$, and the former (NO_2^\bullet) was further converted to NO_2^- under photolysis and finally to N_2 after reaction with $\text{CO}_2^{\bullet-}$ (Equations (3), (6), (7), (9), and (10)). On the other hand, NO_3^- was directly reduced to NH_4^+ or N_2 by $\text{CO}_2^{\bullet-}$ (Equations (11) and (12)) as shown in Scheme 1. Additionally, to confirm the reaction mechanisms of NO_3^- , we further investigated the variation in solution pH over time in UV/ $\text{C}_2\text{O}_4^{2-}$ /Fe³⁺ systems. The results show that the solution pH declined rapidly after the addition of oxalic acids, followed by a gradual increase in the pH over time. For instance, the solution pH was decreased from 7.0 to 2.4 after a dose of oxalic acid was added but increased from 2.4 to 5.7 with increasing time for a total reaction time of 180 min, as illustrated in Figure S7. The consumption of H^+ was consistent with the proposed reduction pathway, as shown in Equations (10)–(12) of Scheme 1. Although $\text{CO}_2^{\bullet-}$ reacted with a small amount of dissolved oxygen in the solution, the generated $\text{O}_2^{\bullet-}$ further oxidized Fe²⁺ to Fe³⁺ (Scheme 1), thus substantiating a minor effect of DO, as shown in Figure 4g.

3.4. The Reduction of Nitrate from Stimulated Groundwater

3.4.1. The Effect of Water Background Compounds

Figure 6a–c show the effect of common anions, such as Cl^- , SO_4^{2-} , and HCO_3^- , during the UV/ $\text{C}_2\text{O}_4^{2-}$ /Fe³⁺ process. The presence of 0.1–10 mM Cl^- or SO_4^{2-} negligibly affected NO_3^- reduction after 180 min, demonstrating the effectiveness of UV/ $\text{C}_2\text{O}_4^{2-}$ /Fe³⁺ systems in the Cl^- - and SO_4^{2-} -containing water matrices. In contrast, HCO_3^- exhibited an inhibitory effect on NO_3^- reduction. There was little impact on NO_3^- reduction at 0–1 mM HCO_3^- , as illustrated in Figure 6c. However, as the HCO_3^- level increased to 10 mM, the reduction efficiency of NO_3^- was decreased by ~10%, which is consistent with previous studies by Gu et al. [31], because HCO_3^- can compete for $\text{CO}_2^{\bullet-}$ with NO_3^- . On the other hand, Figure 6d shows the effect of humic acids (HA). The HA concentration inhibited NO_3^- reduction. With HA concentrations of 0, 10, 20, and 30 mg-C/L, the removal efficiency of NO_3^- was 91.4%, 78.3%, 76.5%, and 61.6%, respectively, after 180 min in the UV/ $\text{C}_2\text{O}_4^{2-}$ /Fe³⁺ process. The inhibitory results are probably due to competitive adsorption of UV light by HA, as well as possible quenching reactions with $\text{CO}_2^{\bullet-}$. In particular, the former prohibited both direct photolysis and radical-induced photocatalysis, and the latter inhibited photocatalysis. Therefore, UV/ $\text{C}_2\text{O}_4^{2-}$ /Fe³⁺ systems could be inhibited in the presence of high HA and HCO_3^- concentrations.

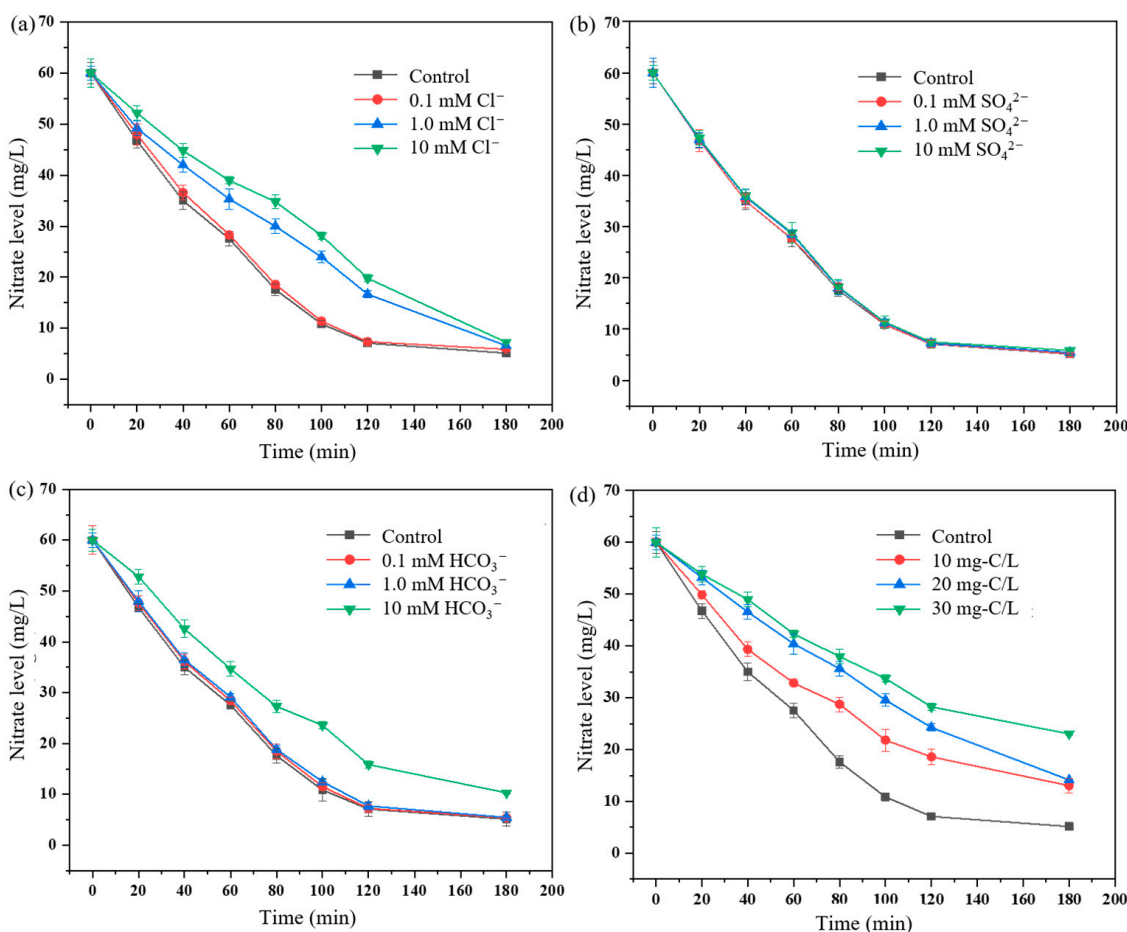


Figure 6. The effect of concentrations of (a) Cl^- (0, 0.1, 1.0, and 10 mM), (b) SO_4^{2-} (0, 0.1, 1.0, and 10 mM), and (c) HCO_3^- (0, 0.1, 1.0, and 10 mM), as well as the effect of (d) humic acids (0, 10, 20, and 30 mg-C/L) on NO_3^- reduction in the $\text{UV}/\text{C}_2\text{O}_4^{2-}/\text{Fe}^{3+}$ process. Experimental conditions: $[\text{NO}_3^-]_0 = 60 \text{ mg/L}$, $[\text{C}_2\text{O}_4^{2-}]_0 = 3 \text{ mM}$, $[\text{Fe}^{3+}]_0 = 0.05 \text{ mM}$, $I_0 = 10.2 \text{ mW/cm}^2$ (wavelength = 365 nm), $[\text{DO}]_0 = 0.5 \pm 0.1 \text{ mg/L}$, $\text{pH}_{\text{ini.}} = 7.0 \pm 0.2$, and $T = 25 \pm 0.5^\circ\text{C}$. Error bars represent the standard deviation from three experiments. Error bars smaller than symbols are not visible.

3.4.2. The Reduction of Nitrate from Simulated Groundwater

To evaluate the effectiveness of $\text{UV}/\text{C}_2\text{O}_4^{2-}/\text{Fe}^{3+}$ systems for NO_3^- reduction in real water, NO_3^- reduction was further performed in simulated groundwater, the characteristics of which were based on inorganic and organic levels in groundwater in Northwest China in Table S1. Figure 7 further presents the reduction of NO_3^- by $\text{UV}/\text{C}_2\text{O}_4^{2-}/\text{Fe}^{3+}$ systems for an initial nitrate concentration of 120 mg NO_3^-/L in simulated groundwater (SGW). There was a slower reduction of NO_3^- in SGW (removal rates = 72.8%) in comparison with deionized water (removal rates = 91.4%) after 180 min at a low DO of 0.5 mg/L (Figures 2 and 3f). This was mainly due to the decreased information of $\text{CO}_2\bullet^-$ resulting from its reaction with inorganic anions (i.e., 122 mg/L HCO_3^-) and strong competitive adsorption of UV light by organic matters, as illustrated in Figure 6. Despite this fact, the NO_3^- concentration decreased to 44.1, 32.6, and 31.0 mg NO_3^-/L after a reaction time of 120, 180, and 240 min, respectively, meeting the drinking water standard (<10 mg/L N- NO_3^- , that is, 44.3 mg NO_3^-/L). In conclusion, the $\text{UV}/\text{C}_2\text{O}_4^{2-}/\text{Fe}^{3+}$ systems are a promising treatment technology as a novel photocatalytic process for efficient and selective decontamination of NO_3^- from complex water matrices.

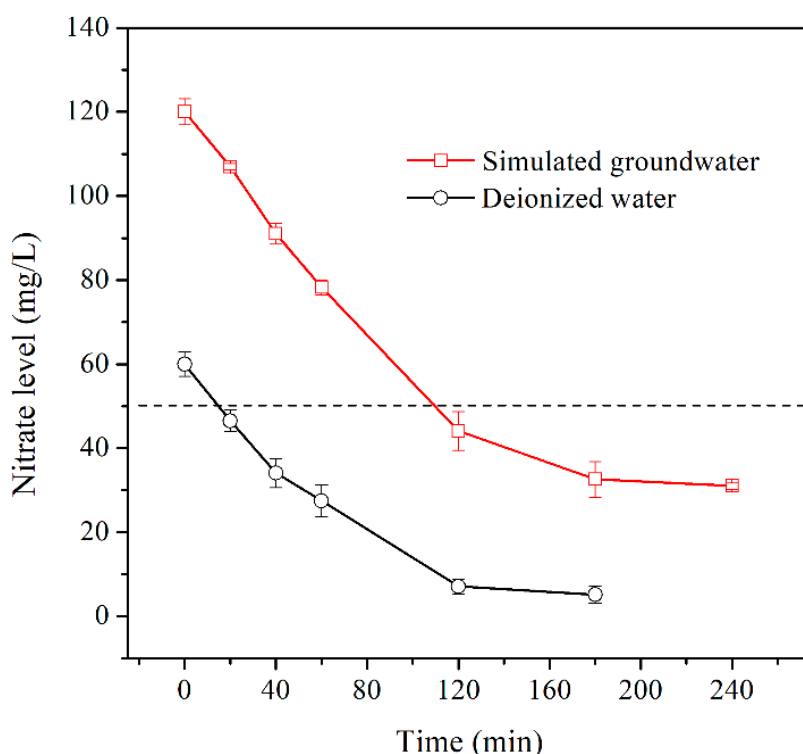


Figure 7. The reduction of NO_3^- from simulated groundwater and deionized water in the $\text{UV}/\text{C}_2\text{O}_4^{2-}/\text{Fe}^{3+}$ process. Experimental conditions: $[\text{NO}_3^-]_0 = 60$ or 120 mg/L , $[\text{C}_2\text{O}_4^{2-}]_0 = 3 \text{ mM}$, $[\text{Fe}^{3+}]_0 = 0.05 \text{ mM}$, $I_0 = 10.2 \text{ mW/cm}^2$ (wavelength = 365 nm), $[\text{DO}]_0 = 0.5 \pm 0.1 \text{ mg/L}$, $\text{pH}_{\text{ini.}} = 7.0 \pm 0.2$, and $T = 25 \pm 0.5 \text{ }^\circ\text{C}$. Error bars represent the standard deviation from three experiments. Error bars smaller than symbols are not visible.

4. Conclusions

The $\text{UV}/\text{C}_2\text{O}_4^{2-}/\text{Fe}^{3+}$ systems have been demonstrated to be an alternative technology for efficient and selective reduction of NO_3^- in water. This system reduced 91.4% of 60 mg/L NO_3^- with a gaseous nitrogen selectivity of 84.2% in 180 min, compared to UV alone, $\text{UV}/\text{C}_2\text{O}_4^{2-}$ systems, and UV/Fe^{3+} processes. The quenching experiment demonstrated that $\text{CO}_2\bullet^-$ was primarily responsible for NO_3^- reduction. Further, the mass balance calculation of nitrogen, carbon, and iron showed that NH_4^+ , N_2 , CO_2 , and Fe^{2+} were the primary reaction products. Reduction pathways were proposed accordingly. Appropriate oxalic acids levels (i.e., 3 mM) and initial NO_3^- doses (i.e., 60 mg/L) facilitated NO_3^- reduction and gaseous nitrogen conversion. The higher the Fe^{3+} concentration and UV intensity are, the greater the reduction of NO_3^- is. A higher initial pH inhibited NO_3^- reduction due to the lower proportion of iron (III)-oxalate at higher pHs. Of note, $0.5\text{--}8.0 \text{ mg/L}$ of dissolved oxygen did not have a significant inhibitory effect. Comparatively, the $\text{UV}/\text{C}_2\text{O}_4^{2-}/\text{Fe}^{3+}$ systems were not inhibited by $0.1\text{--}10 \text{ mM}$ Cl^- or SO_4^{2-} or $0.1\text{--}1.0 \text{ mM}$ HCO_3^- but was retarded by 10 mM HCO_3^- . Additionally, 30 mg-C/L humic acid (HA) led to the decreased NO_3^- reduction, probably because of competitive UV adsorption by HA, and its possible reactions with $\text{CO}_2\bullet^-$. As expected, NO_3^- reduction in simulated groundwater was not as fast as in deionized water, mainly due to the presence of competing anions (i.e., HCO_3^-) and natural organic matters (i.e., HA) in complex water matrices. Moreover, considering its cost-effectiveness and the wide availability of reagents in nature (i.e., iron and oxalic acid), $\text{UV}/\text{C}_2\text{O}_4^{2-}/\text{Fe}^{3+}$ systems are particularly attractive in the selective and effective conversion of NO_3^- to N_2 . Overall, the $\text{UV}/\text{C}_2\text{O}_4^{2-}/\text{Fe}^{3+}$ process is an alternative selective reduction technology in the field of environmental water treatment.

Supplementary Materials: The following supporting information can be downloaded at: <https://www.mdpi.com/article/10.3390/catal12030348/s1>, Figure S1: Mineralization of oxalic acid in the UV/C₂O₄²⁻/Fe³⁺ systems; Figure S2: Formation of primary products at different dosage of oxalate acids during reduction of NO₃⁻ in the UV/C₂O₄²⁻/Fe³⁺ systems; Figure S3: Formation of primary products at different initial Fe³⁺ levels during reduction of NO₃⁻ in the UV/C₂O₄²⁻/Fe³⁺ systems; Figure S4: The ln(C₀/C) value versus reaction time at various solution pH in the UV/C₂O₄²⁻/Fe³⁺ systems; Figure S5: Formation of primary products at different UV lamp power during reduction of NO₃⁻ in the UV/C₂O₄²⁻/Fe³⁺ systems; Figure S6: Formation of primary products at various initial NO₃⁻ levels during reduction of NO₃⁻ in the UV/C₂O₄²⁻/Fe³⁺ systems; Figure S7: The variation of solution pH with time in the UV/C₂O₄²⁻/Fe³⁺ systems; Table S1: The characteristics of simulated groundwater; Table S2: Kinetic parameters of NO₃⁻ reduction at various Fe³⁺ levels; Table S3: Kinetic parameters of NO₃⁻ reduction at different initial solution pH; Table S4: Kinetic parameters of NO₃⁻ reduction at different UV light intensity.

Author Contributions: Conceptualization, Z.S. and F.W.; methodology, F.W.; software, F.W.; validation, Z.S., F.W. and X.J.; formal analysis, Z.S.; investigation, Z.S.; resources, F.W.; data curation, X.J.; writing—original draft preparation, Q.X.; writing—review and editing, Q.X. and S.Y.; visualization, Q.X. and S.Y.; supervision, S.Y.; project administration, Q.X. and S.Y.; funding acquisition, S.Y. All authors have read and agreed to the published version of the manuscript.

Funding: This research was funded by the National Natural Science Foundation of China grant number 51978484.

Conflicts of Interest: The authors declare no conflict of interest.

Sample Availability: Samples of the compounds are not available from the authors upon request.

References

1. Garcia-Segura, S.; Lanzarini-Lopes, M.; Hristovski, K.; Westerhoff, P. Electrocatalytic reduction of nitrate: Fundamentals to full-scale water treatment applications. *Appl. Catal. B Environ.* **2018**, *236*, 546–568. [[CrossRef](#)]
2. Doudrick, K.; Yang, T.; Hristovski, K.; Westerhoff, P. Photocatalytic nitrate reduction in water: Managing the hole scavenger and reaction by-product selectivity. *Appl. Catal. B Environ.* **2013**, *136–137*, 40–47. [[CrossRef](#)]
3. Hamlin, H.J. Nitrate toxicity in Siberian sturgeon (*Acipenser baeri*). *Aquaculture* **2006**, *253*, 688–693. [[CrossRef](#)]
4. Hamlin, H.J.; Moore, B.C.; Edwards, T.M.; Larkin, I.L.V.; Boggs, A.; High, W.J.; Main, K.L.; Guillette, L.J. Nitrate-induced elevations in circulating sex steroid concentrations in female Siberian sturgeon (*Acipenser baeri*) in commercial aquaculture. *Aquaculture* **2008**, *281*, 118–125. [[CrossRef](#)]
5. Zhang, W.L.; Tian, Z.X.; Zhang, N.; Li, X.Q. Nitrate pollution of groundwater in northern China. *Agric. Ecosyst. Environ.* **1996**, *59*, 223–231. [[CrossRef](#)]
6. Ashok, V.; Hait, S. Remediation of nitrate-contaminated water by solid-phase denitrification process—a review. *Environ. Sci. Pollut. Res. Int.* **2015**, *22*, 8075–8093. [[CrossRef](#)] [[PubMed](#)]
7. Zhong, Y.; Li, X.; Yang, Q.; Wang, D.; Yao, F.; Li, X.; Zhao, J.; Xu, Q.; Zhang, C.; Zeng, G. Complete bromate and nitrate reduction using hydrogen as the sole electron donor in a rotating biofilm-electrode reactor. *J. Hazard. Mater.* **2016**, *307*, 82–90. [[CrossRef](#)]
8. Dong, L.; Lin, L.; Li, Q.; Huang, Z.; Tang, X.; Wu, M.; Li, C.; Cao, X.; Scholz, M. Enhanced nitrate-nitrogen removal by modified attapulgite-supported nanoscale zero-valent iron treating simulated groundwater. *J. Environ. Manag.* **2018**, *213*, 151–158. [[CrossRef](#)]
9. Ma, X.; Li, M.; Liu, X.; Wang, L.; Chen, N.; Li, J.; Feng, C. A graphene oxide nanosheet-modified Ti nanocomposite electrode with enhanced electrochemical property and stability for nitrate reduction. *Chem. Eng. J.* **2018**, *348*, 171–179. [[CrossRef](#)]
10. Rao, X.; Shao, X.; Xu, J.; Yi, J.; Qiao, J.; Li, Q.; Wang, H.; Chien, M.; Inoue, C.; Liu, Y.; et al. Efficient nitrate removal from water using selected cathodes and Ti/PbO₂ anode: Experimental study and mechanism verification. *Sep. Purif. Technol.* **2019**, *216*, 158–165. [[CrossRef](#)]
11. Liu, G.; You, S.; Ma, M.; Huang, H.; Ren, N. Removal of Nitrate by Photocatalytic Denitrification Using Nonlinear Optical Material. *Environ. Sci. Technol.* **2016**, *50*, 11218–11225. [[CrossRef](#)] [[PubMed](#)]
12. de Bem Luiz, D.; Andersen, S.L.F.; Berger, C.; José, H.J.; Moreira, R.d.F.P.M. Photocatalytic reduction of nitrate ions in water over metal-modified TiO₂. *J. Photochem. Photobiol. A Chem.* **2012**, *246*, 36–44. [[CrossRef](#)]
13. Petsi, P.N.; Saradis, V.C.; Plakas, K.V.; Karabelas, A.J. Reduction of nitrates in a photocatalytic membrane reactor in the presence of organic acids. *J. Environ. Manag.* **2021**, *298*, 113526. [[CrossRef](#)] [[PubMed](#)]
14. Opbergen, G.; Peters, T.; Rautenbach, R.; Tils, H. Reduction of nitrate concentration in drinking water by a hybrid process with zero discharge based on reverse osmosis. *Desalination* **1983**, *47*, 267–274. [[CrossRef](#)]
15. Huang, X.; Wang, L.; Zhou, J.; Gao, N. Photocatalytic decomposition of bromate ion by the UV/P25-graphene processes. *Water Res.* **2014**, *57*, 1–7. [[CrossRef](#)]

16. Xiao, Q.; Ren, Y.; Yu, S. Pilot study on bromate reduction from drinking water by UV/sulfite systems: Economic cost comparisons, effects of environmental parameters and mechanisms. *Chem. Eng. J.* **2017**, *330*, 1203–1210. [[CrossRef](#)]
17. Xiao, Q.; Yu, S.; Li, L.; Wang, T.; Liao, X.; Ye, Y. An overview of advanced reduction processes for bromate removal from drinking water: Reducing agents, activation methods, applications and mechanisms. *J. Hazard. Mater.* **2017**, *324*, 230–240. [[CrossRef](#)]
18. Xiao, Q.; Yu, S.; Li, L.; Zhang, Y.; Yi, P. Degradation of bromate by Fe(II)-Ti(IV) layered double hydroxides nanoparticles under ultraviolet light. *Water Res.* **2019**, *150*, 310–320. [[CrossRef](#)]
19. Tugaoen, H.O.; Garcia-Segura, S.; Hristovski, K.; Westerhoff, P. Challenges in photocatalytic reduction of nitrate as a water treatment technology. *Sci. Total Environ.* **2017**, *599*–*600*, 1524–1551. [[CrossRef](#)]
20. Nawaz, S.; Shah, N.S.; Khan, J.A.; Sayed, M.; Al-Muhtaseb, A.a.H.; Andersen, H.R.; Muhammad, N.; Murtaza, B.; Khan, H.M. Removal efficiency and economic cost comparison of hydrated electron-mediated reductive pathways for treatment of bromate. *Chem. Eng. J.* **2017**, *320*, 523–531. [[CrossRef](#)]
21. Herrmann, H. On the photolysis of simple anions and neutral molecules as sources of O^- /OH, SO_x^- and Cl in aqueous solution. *Phys. Chem. Chem. Phys.* **2007**, *9*, 3935–3964. [[CrossRef](#)] [[PubMed](#)]
22. Lian, R.; Oulianov, D.A.; Crowell, R.A.; Shkrob, I.A.; Chen, X.; Bradforth, S.E. Electron photodetachment from aqueous anions. 3. Dynamics of geminate pairs derived from photoexcitation of mono- vs polyatomic anions. *J. Phys. Chem. A* **2006**, *110*, 9071–9078. [[CrossRef](#)] [[PubMed](#)]
23. Xiao, Q.; Wang, T.; Yu, S.; Yi, P.; Li, L. Influence of UV lamp, sulfur(IV) concentration, and pH on bromate degradation in UV/sulfite systems: Mechanisms and applications. *Water Res.* **2017**, *111*, 288–296. [[CrossRef](#)]
24. Vellanki, B.P.; Batchelor, B. Perchlorate reduction by the sulfite/ultraviolet light advanced reduction process. *J. Hazard. Mater.* **2013**, *262*, 348–356. [[CrossRef](#)] [[PubMed](#)]
25. Im, J.K.; Son, H.S.; Zoh, K.D. Perchlorate removal in Fe^0/H_2O systems: Impact of oxygen availability and UV radiation. *J. Hazard. Mater.* **2011**, *192*, 457–464. [[CrossRef](#)]
26. Jung, B.; Sivasubramanian, R.; Batchelor, B.; Abdel-Wahab, A. Chlorate reduction by dithionite/UV advanced reduction process. *Int. J. Environ. Sci. Technol.* **2016**, *14*, 123–134. [[CrossRef](#)]
27. Vellanki, B.P.; Batchelor, B.; Abdel-Wahab, A. Advanced reduction processes: A new class of treatment processes. *Environ. Eng. Sci.* **2013**, *30*, 264–271. [[CrossRef](#)]
28. Li, X.; Ma, J.; Liu, G.; Fang, J.; Yue, S.; Guan, Y.; Chen, L.; Liu, X. Efficient reductive dechlorination of monochloroacetic acid by sulfite/UV process. *Environ. Sci. Technol.* **2012**, *46*, 7342–7349. [[CrossRef](#)]
29. Chaplin, B.P.; Reinhard, M.; Schneider, W.F.; Schuth, C.; Shapley, J.R.; Strathmann, T.J.; Werth, C.J. Critical review of Pd-based catalytic treatment of priority contaminants in water. *Environ. Sci. Technol.* **2012**, *46*, 3655–3670. [[CrossRef](#)]
30. Liu, X.; Zhong, J.; Fang, L.; Wang, L.; Ye, M.; Shao, Y.; Li, J.; Zhang, T. Trichloroacetic acid reduction by an advanced reduction process based on carboxyl anion radical. *Chem. Eng. J.* **2016**, *303*, 56–63. [[CrossRef](#)]
31. Gu, X.; Lu, S.; Fu, X.; Qiu, Z.; Sui, Q.; Guo, X. Carbon dioxide radical anion-based UV/ $S_2O_8^{2-}$ /HCOOH reductive process for carbon tetrachloride degradation in aqueous solution. *Sep. Purif. Technol.* **2017**, *172*, 211–216. [[CrossRef](#)]
32. Zhou, Q.; Niu, W.; Li, Y.; Li, X. Photoinduced Fenton-simulated reduction system based on iron cycle and carbon dioxide radicals production for rapid removal of Cr(VI) from wastewater. *J. Clean. Prod.* **2020**, *258*, 120790. [[CrossRef](#)]
33. Berkovic, A.M.; Bertolotti, S.G.; Villata, L.S.; Gonzalez, M.C.; Diez, R.P.; Martire, D.O. Photoinduced reduction of divalent mercury by quinones in the presence of formic acid under anaerobic conditions. *Chemosphere* **2012**, *89*, 1189–1194. [[CrossRef](#)]
34. Chen, G.; Hanukovich, S.; Chebeir, M.; Christopher, P.; Liu, H. Nitrate removal via a formate radical-induced photochemical process. *Environ. Sci. Technol.* **2019**, *53*, 316–324. [[CrossRef](#)] [[PubMed](#)]
35. An, B.; He, H.; Duan, B.; Deng, J.; Liu, Y. Selective reduction of nitrite to nitrogen gas by CO_2 anion radical from the activation of oxalate. *Chemosphere* **2021**, *278*, 130388. [[CrossRef](#)] [[PubMed](#)]
36. Liu, X.; Zhang, T.; Shao, Y. Aqueous bromate reduction by UV activation of sulfite. *Clean-Soil Air Water* **2014**, *42*, 1370–1375. [[CrossRef](#)]
37. Dong, H.; Wei, G.; Yin, D.; Guan, X. Mechanistic insight into the generation of reactive oxygen species in sulfite activation with Fe(III) for contaminants degradation. *J. Hazard. Mater.* **2020**, *384*, 121497. [[CrossRef](#)]
38. Xiao, Q.; Yu, S. The role of dissolved oxygen in the sulfite/divalent transition metal ion system: Degradation performances and mechanisms. *Chem. Eng. J.* **2021**, *417*, 129115. [[CrossRef](#)]
39. Wang, L.; Fu, W.; Zhuge, Y.; Wang, J.; Yao, F.; Zhong, W.; Ge, X. Synthesis of polyoxometalates (POM)/ TiO_2/Cu and removal of nitrate nitrogen in water by photocatalysis. *Chemosphere* **2021**, *278*, 130298. [[CrossRef](#)]
40. Kobwittaya, K.; Sirivithayapakorn, S. Photocatalytic reduction of nitrate over TiO_2 and Ag-modified TiO_2 . *J. Saudi Chem. Soc.* **2014**, *18*, 291–298. [[CrossRef](#)]
41. Rosso, J.A.; Bertolotti, S.G.; Braun, A.M.; Martire, D.O.; Gonzalez, M.C. Reactions of carbon dioxide radical anion with substituted benzenes. *J. Phys. Org. Chem.* **2001**, *14*, 300–309. [[CrossRef](#)]
42. Balmer, M.E.; Sulzberger, B. Atrazine Degradation in Irradiated Iron/Oxalate Systems: Effects of pH and Oxalate. *Environ. Sci. Technol.* **1999**, *33*, 2418–2424. [[CrossRef](#)]
43. Tachikawa, T.; Tojo, S.; Fujitsuka, M.; Majima, T. Direct observation of the one-electron reduction of Methyl Viologen mediated by the CO_2 radical anion during TiO_2 photocatalytic reactions. *Langmuir ACS J. Surf. Colloids* **2004**, *20*, 9441–9444. [[CrossRef](#)] [[PubMed](#)]

44. Mazarji, M.; Kuthiala, S.; Tsapekos, P.; Alvarado-Morales, M.; Angelidaki, I. Carbon dioxide anion radical as a tool to enhance lignin valorization. *Sci. Total Environ.* **2019**, *682*, 47–58. [[CrossRef](#)]
45. Buresh, R.J.; Moraghan, J.T. Chemical reduction of nitrate by ferrous iron. *J. Environ. Qual.* **1976**, *5*, 320–325. [[CrossRef](#)]
46. Mulazzani, Q.G.; D’Angelantonio, M.; Venturi, M.; Hoffman, M.Z.; Rodgers, M.A.J. Interaction of formate and oxalate ions with radiation-generated radicals in aqueous solution. Methylviologen as a mechanistic probe. *J. Phys. Chem.* **1986**, *90*, 5347–5352. [[CrossRef](#)]